Multiwall Carbon Nanotube and Poly(3,4-ethylenedioxythiophene): Polystyrene Sulfonate (PEDOT:PSS) Composite Films for Transistor and Inverter Devices

Dong-Jin Yun, KiPyo Hong, Se hyun Kim, Won-Min Yun, Jae-young Jang, Woo-Sung Kwon, Chan-Eon Park, and Shi-Woo Rhee*

System on Chip Chemical Process Research Center, Department of Chemical Engineering, Pohang University of Science and Technology (POSTECH), Pohang 790-784, Korea

ABSTRACT Highly conductive multiwalled carbon nanotube (MWNT)/Poly(3,4-ethylenedioxythiophene) polymerized with poly(4-styrenesulfonate) (PEDOT:PSS) films were prepared by spin coating a mixture solution. The solution was prepared by dispersing MWNT in the PEDOT:PSS solution in water using ultrasonication without any oxidation process. The effect of the MWNT loading in the solution on the film properties such as surface roughness, work function, surface energy, optical transparency, and conductivity was studied. The conductivity of MWNT/PEDOT:PSS composite film was increased with higher MWNT loading and the high conductivity of MWNT/PEDOT:PSS films enabled them to be used as a source/drain electrode in organic thin film transistor (OTFT). The pentacene TFT with MWNT/PEDOT:PSS S/D electrode showed much higher performance with mobility about 0.2 $cm^2/(V\ s)$ and on/off ratio about 5×10^5 compared to that with PEDOT:PSS S/D electrode (~0.05 $cm^2/(V\ s)$, 1×10^5). The complementary inverters exhibited excellent characteristics, including high gain value of about 30.

KEYWORDS: MWNT • PEDOT:PSS • MWNT/PEDOT:PSS composite film • organic thin film transistor • inverter

1. INTRODUCTION

Many groups have studied electrode materials for electronic devices including organic thin film transistor (OTFT), organic photovoltaic (OPV), dye sensitized solar cell (DSSC), organic light emitting diode (OLED) to improve the device performance with low-cost materials and processes (1−4). Carbon nano tube (CNT) is an attractive candidate for this application due to its high conductivity, stability and optical transmittance (3, 5−8). CNT material has been applied in various fields including OLED, OTFT, OPV, and DSSC as an emitting, catalytic or transparent electrode s (9−12). CNT, however, has an intrinsic problem of insolubility in most solvents and many groups have tried to solve this problem in decades (13, 14). The oxidation of CNT and grafting of polymer onto CNT are the most widely utilized methods to improve the solubility of CNT in solvents (13−16). Although the oxidized CNT dissolves well in polar solvents such as ethanol and water because of the introduction of −OH and −COOH functional groups, the conductivity of oxidized CNT is much poorer compared to bare CNT (16−18). In contrast, the polymer grafting onto CNT can improve the solubility of CNT without the conductivity loss and the conductivity of the film can be further improved in combination with highly conductive polymer (19, 20). Among them, poly(3,4-ethylenedioxythiophene) polymerized with poly(4-styrenesulfonate) (PEDOT:PSS) is the potent candidate because of the high conductivity (0.1 to 1×10^5 S/cm) and solubility in polar solvent (21−23). On the basis of these advantages, studies on the application of CNT, PEDOT:PSS or CNT/PEDOT:PSS composite films as an electrode of OLED and catalytic counter electrode (CCE) of DSSC have been reported in recent years, but so far, there have been few reports on the effect of CNT/PEDOT:PSS composition on the film properties or on the performance analysis of CNT/PEDOT:PSS nanocomposites as an electrode material in OTFT, OLED, or DSSC.

In this work, without the oxidation process of MWNT, MWNT/PEDOT:PSS composite solutions with various compositions were prepared and MWNT/PEDOT:PSS composite films were prepared with spin-coating on SiO_2 (300 nm) surface thermally grown on Si substrate. The film properties such as resistivity, work function, morphology, and surface energy were measured. The pentacene TFTs and complementary inverters with MWNT/PEDOT:PSS source/drain (S/D) electrode were fabricated and their performance was characterized.

2. EXPERIMENTAL SECTION

PEDOT:PSS solution (CLEVIOS PH500: 1 wt % in water) and MWNT were purchased from H.C. Starck and Carbon Nanomaterial Technology Co., respectively. As-purchased MWNT was dispersed in diluted PEDOT:PSS solution using only ultrasonication and without functionalization of MWNT. MWNT was dispersed well and the MWNT/PEDOT:PSS solution remained without sediment for more than a week. Various amount of MWNTs (0.05, 0.1, 0.15, 0.2, and 0.3 g) were dissolved in the

* E-mail: srhee@postech.ac.kr. Tel: 82-54-279-2265. Fax: 82-54-279-8619.
Received for review September 5, 2010 and accepted November 27, 2010

DOI: 10.1021/am1008375

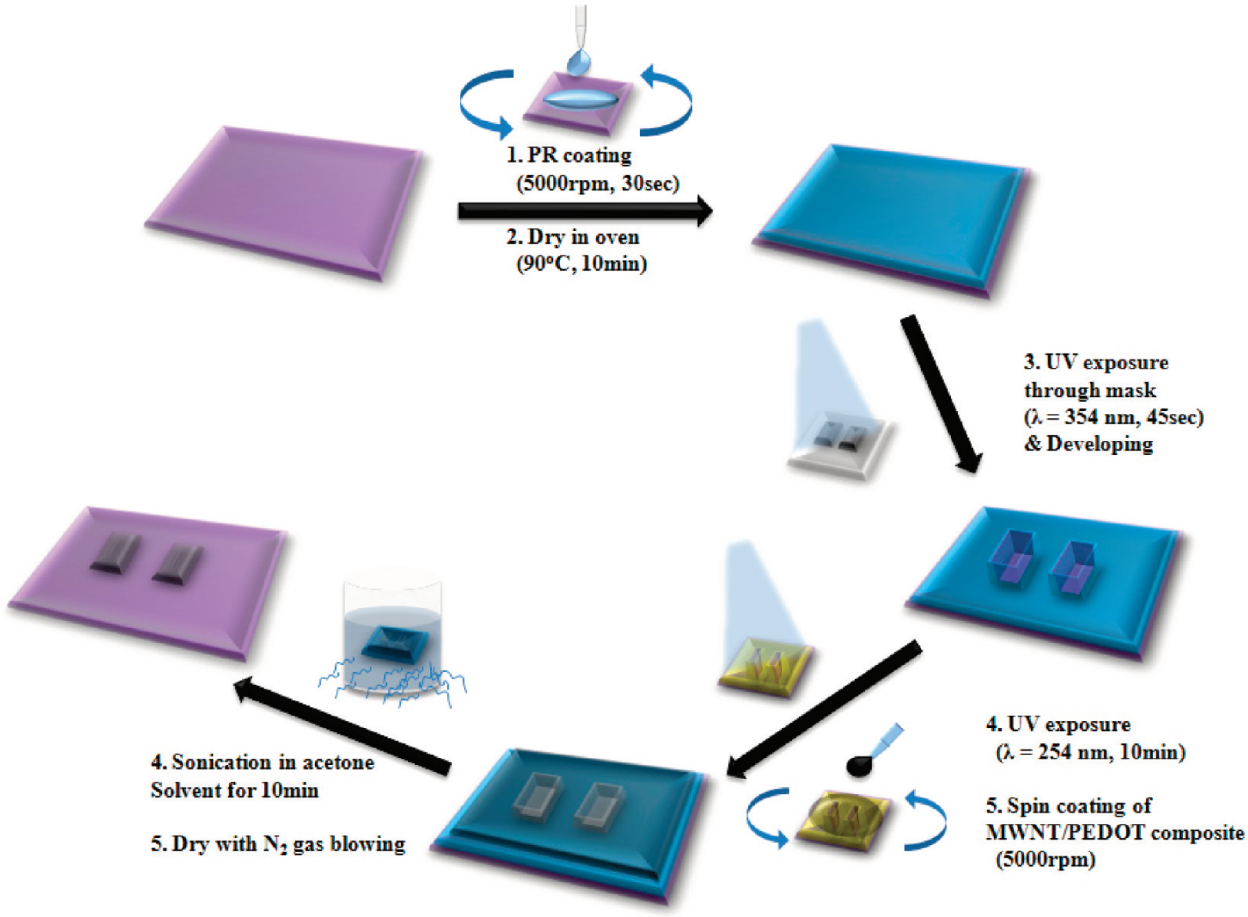

FIGURE 1. Patterning process of the MWNT/PEDOT:PSS film to be used as an S/D electrode in OTFT.

mixture of PEDOT:PSS solution (10 mL) and deionized (DI) water (10 mL) with ultrasonication for 30 min using high-intensity ultrasonic probe (Ulsso Hitech Co., Korea, Ti-Horn, 19.87 kHz, 700 W). In this paper, 0.2 MWNT implies the mixture of 0.985 wt % MWNT and 0.49 wt % PEDOT:PSS in 20 mL of water. MWNT/PEDOT:PSS composite films were prepared using spin-coating (5000 rpm) of the MWNT/PEDOT:PSS solution on SiO_2 (300 nm)/N++Si substrate (Silicon Material Inc.) and then annealed in a vacuum oven at ~100 °C for 2 h.

The pentacene TFTs with MWNT/PEDOT:PSS S/D electrodes were fabricated and the performance was measured. OTS (octadecyltrichlorosilane) monolayer was formed on the oxide surface to improve the interface property of pentacene on insulator (1). Prior to the formation of OTS monolayer, SiO_2 (300 nm)/N+Si substrate was dipped in piranha solution (H_2SO_4:H_2O_2 = 7:4 vol %) for 1 h at ~100 °C and cleaned in UV tip cleaner (UV TC 220, PUCOTECH) for 30 min. Then, cleaned substrate was dipped in the 1 mM OTS-toluene (purchased from Aldrich Chemical Co.) solution for 2 h at low temperature of ~4 °C and washed out in toluene and acetone for 30 min each with sonication. Finally, OTS treated substrate was annealed in a vacuum chamber for 2 h at 150 °C and kept in a vacuum chamber at 50 °C.

The lift-off process was used to pattern the S/D electrode of the pentacene TFT. Photoresist (negative type PR, AZ5214-E) was spin-coated on the substrate with a speed of 5000 rpm for 45s, then, exposed to UV light of ~350 nm major wavelength through photolithography-mask and then washed out with developer and DI water. Subsequently, the substrate was exposed to UV-ozone in a UV tip cleaner for 10 min and the MWNT/PEDOT:PSS film for S/D electrode was spin-coated (5000 rpm) on the whole substrate surface. The substrate was then annealed in a vacuum oven at ~100 °C for 2 h and washed in acetone with sonication. The patterning process of the MWNT/PEDOT:PSS film to be used as a S/D electrode in OTFT was briefly summarized in Figure 1. Pentacene films as an organic semiconductor in OTFTs were deposited at 70 °C with a deposition rate of 0.2−0.3 Å/s in an organic molecular beam deposition (OMBD) system at a pressure of 2×10^{-6} Torr. The same procedures were used to fabricate an inverter (channel length: 100 μm and channel width: 1000 μm). *N*,*N*′-Ditridecyl perylene diimide (PTCDI-C13) films were deposited at room temperature with a rate of 0.2−0.3 ÅA/s in an OMBD system.

The sheet resistance of MWNT/PEDOT:PSS films was measured with 4-point probe method (KEITHLEY 2400 sourcemeter) and the top-view of S/D electrodes patterned using photolithography were observed with optical microscope (OM). The morphology of MWNT/PEDOT:PSS films was investigated using atomic force measurement (AFM, Veeco Nanoscope V in NCNT) and secondary emission microscope (SEM, JEOL JSM-7401F). The bonding state and work function of MWNT/PEDOT:PSS films were investigated with X-ray photoemission spectroscopy (XPS) and ultraviolet photoemission spectroscopy (UPS) measurement. The current−voltage (I−V) characteristics of the pentacene TFT and inverter were measured at room temperature using Agilent E5270A precision semiconductor parameter analyzer and Keithley 4200 semiconductor characterization system.

3. RESULTS AND DISCUSSION

The morphology of the spin-coated MWNT/PEDOT:PSS films were highly dependent on the concentration of the MWNT/PEDOT:PSS solution. Figure 2 shows the compara-

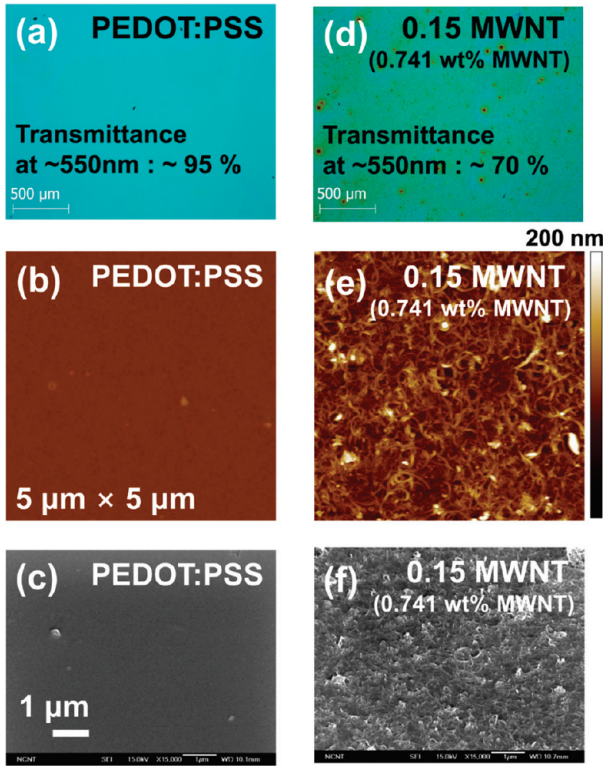

FIGURE 2. Morphology of PEDOT:PSS and 0.15 MWNT/PEDOT:PSS films observed with OM, SEM, and AFM.

tive morphologies (studied by OM, AFM, and SEM measurement) of 0.15 MWNT (0.741 wt % MWNT) composite film. As the concentration of MWNT in MWNT/PEDOT:PSS solution was increased, the packing density of MWNT at the film surface and the film roughness increased. The optical transmittance of PEDOT:PSS film at visible region (wavelength between 400 and 800 nm) shows ~95%, but it was decreased with the increase in the MWNT concentration in the PEDOT:PSS solution and 0.15 MWNT composite film shows the optical transmittance of ~70%. It was believed that the addition of MWNT in the film blocks the light transmission. The surface of the MWNT/PEDOT:PSS film observed with AFM and SEM showed that MWNT were well-dispersed, densely packed, and well-connected with one another as shown in Figure 2 c–f.

The sheet resistance as a function of the amount of MWNT in PEDOT:PSS solution was plotted in Figure 3a. The sheet resistances of the 0.05 MWNT (0.248 wt % MWNT), 0.15 MWNT and 0.3 MWNT (1.47 wt % MWNT) composite films were measured to be ~186 ± 22.5 kΩ/□, 6.9 ± 1.3 kΩ/□, and 734 ± 450 kΩ/□, respectively. The resistivity of PEDOT:PSS film could be decreased with the addition of MWNT in the PEDOT:PSS solution, and the sheet resistance of the MWNT/PEDOT:PSS film was decreased as the amount of MWNT in the PEDOT:PSS solution was

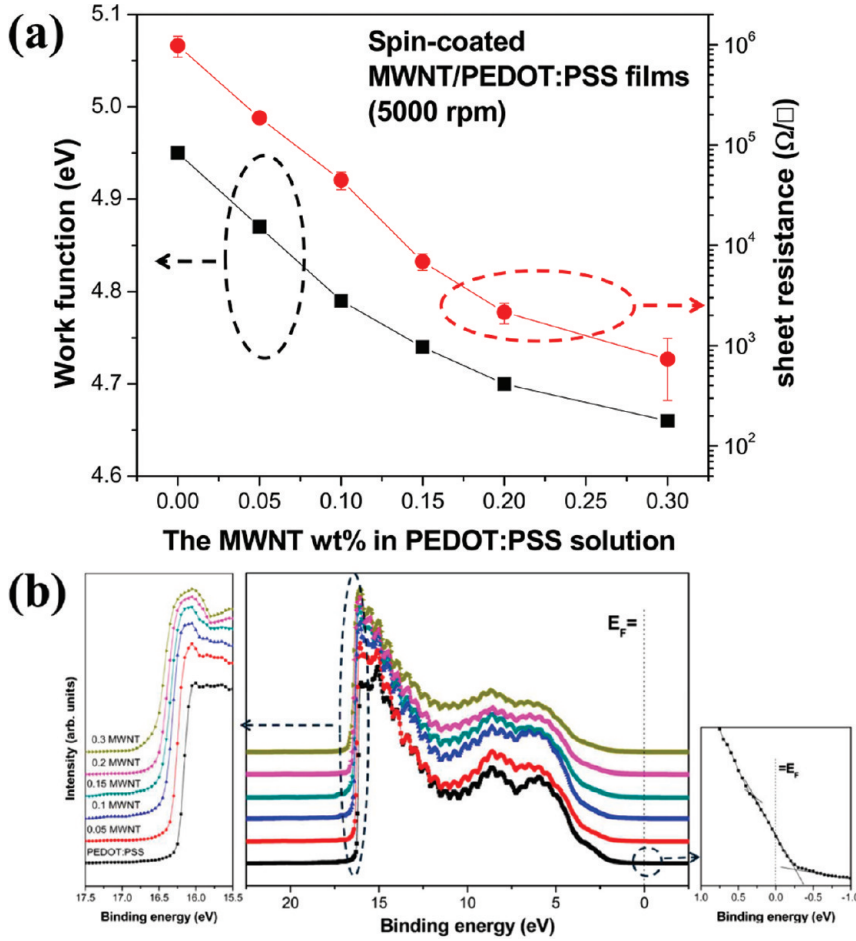

FIGURE 3. (a) Sheet resistance and work function, and (b) the UPS spectrum of the MWNT/PEDOT:PSS film as a function of the MWNT loading in the PEDOT:PSS solution.

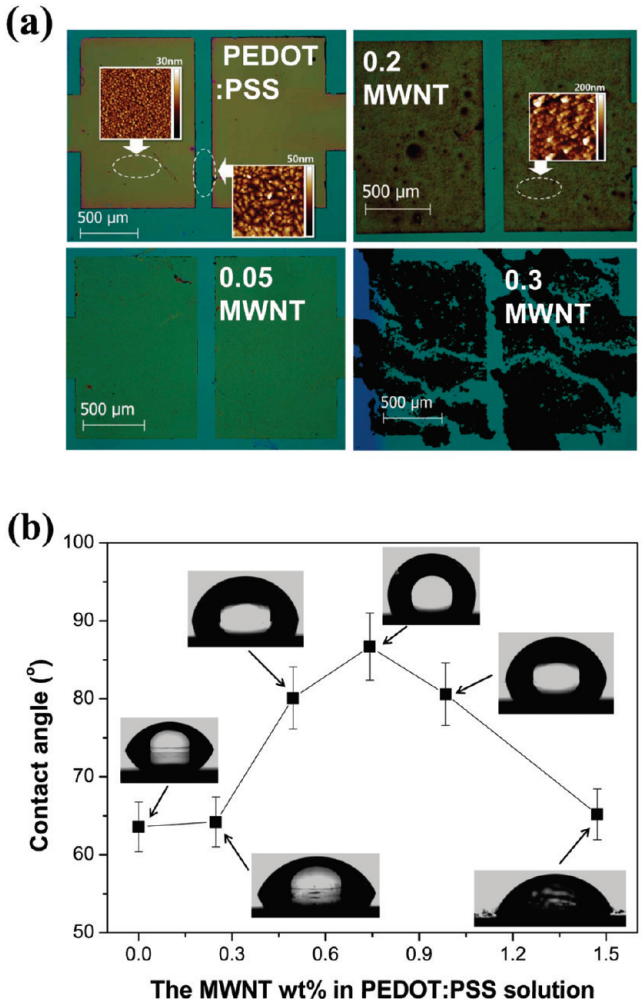

FIGURE 4. (a) OM images near the channel region of pentacene TFTs and (b) the contact angle of DI water on the MWNT/PEDOT:PSS films as a function of the MWNT loading.

increased because of the connectivity enhancement between highly conductive MWNT. Although the PEDOT:PSS film showed high smoothness and transparency, the sheet resistance (~200 kΩ/□) is too high to be used as an electrode material. Figure 3b shows the comparative UPS spectrum of the MWNT/PEDOT:PSS films with various amount of MWNT. The secondary cutoff region (E_{cutoff}) and Fermi energy (E_F) were clearly defined and the work function of MWNT/PEDOT:PSS film was calculated using the following eq 1

$$\phi = h\nu(=21.2\ \text{eV}) - E_{\text{cutoff}} + E_{\text{Fermi}} \qquad (1)$$

Here, $h\nu$ (= 21.2 eV) is the incoming photon energy from He I source and the −5 V bias was applied to make a clear boundary in the E_{cutoff} region. The work function of conductive film highly depends on the surface properties as well as the bulk properties. As observed in the morphological images of 0.15 MWNT, MWNT was densely tangled on the surface and it is believed that the surface properties including work function highly depend on the properties of MWNT as the MWNT loading is increased. The work function of the MWNT/PEDOT:PSS film was decreased from 5.0 eV (pure PEDOT:PSS) down to 4.6 eV (pure MWNT). The work function of the PEDOT:PSS and 0.2 MWNT composite film was measured to be 4.95 and 4.70 eV, respectively. As summarized in Figure 3a, the work function and the sheet resistance showed the same trend and both were attributable to the MWNT density change in the MWNT/PEDOT:PSS composite film.

Figure 4a shows patterned MWNT/PEDOT:PSS S/D electrode and AFM images of pentacene film grown on PEDOT:PSS, 0.2 MWNT and channel region (OTS-treated SiO_2). 0.3 MWNT solution forms gel state because too much MWNT was loaded and the film could not be patterned using lithography process. Below this loading, the MWNT/PEDOT:PSS S/D electrode were well patterned with a channel length of 150 μm and channel width of 1500 μm as shown in Figure 4a. The PEDOT:PSS film showed a low contact angle of ~63 ± 3° with DI water, but 0.1 MWNT (0.495 wt % MWNT), 0.15 MWNT and 0.2 MWNT composite films showed similar contact angle near ~80 ± 5°, as summarized in Figure 4b. As the MWNT loading was increased, the surface energy was decreased and the pentacene film grown on MWNT/PEDOT:PSS film showed slightly larger grain size than on PEDOT:PSS film because of the hydrophobic property of MWNT/PEDOT:PSS films. It was believed that the large grain size of pentacene on MWNT/PEDOT:PSS film would improve hole transport near S/D electrode.

Bottom-contact pentacene TFTs were fabricated using MWNT/PEDOT:PSS films as a S/D electrode. The field-effect mobility in the saturated regime (V_D = −40 V) was calculated using the formula given below

Table 1. Film Properties of the MWNT/PEDOT:PSS Film and the Characteristics of the Pentacene TFT with MWNT/PEDOT:PSS S/D Electrode As a Function of the MWNT Loading

	MWNT/PEDOT:PSS film properties						Characteristics of OTFTs		
materials	MWNT wt % in PEDOT:PSS solution	thickness (nm)	sheet resistivity (Ω/□)	Roughness (nm)	Optical Transmittance at 550 nm (%)	Work Function (Φ)	Field-effect mobility (cm^2/(V s))	On/off current ratio	Threshold voltage (V_{th})
PEDOT:PSS		50	980000 ± 230000	0.815	96.8	4.95	0.0447 ± 0.025	~10^5	1.45 ± 0.2
0.05 MWNT	0.248	100 ± 30	186000 ± 22500	8.5	90.5	4.87	0.0723 ± 0.035	~10^5	−2.38 ± 0.15
0.1 MWNT	0.495	130 ± 40	44800 ± 9000	12	83.2	4.79	0.23 ± 0.04	~5 × 10^5	−4.52 ± 0.37
0.15 MWNT	0.741	150 ± 50	6900 ± 1300	15.9	68.7	4.74	0.208 ± 0.037	~5 × 10^5	−4.95 ± 0.5
0.2 MWNT	0.985	150 ± 50	2150 ± 500	25.4	56.5	4.70	0.236 ± 0.046	~5 × 10^5	−4.4 ± 0.5
0.3 MWNT	1.471		734 ± 450	111	25.5	4.66			

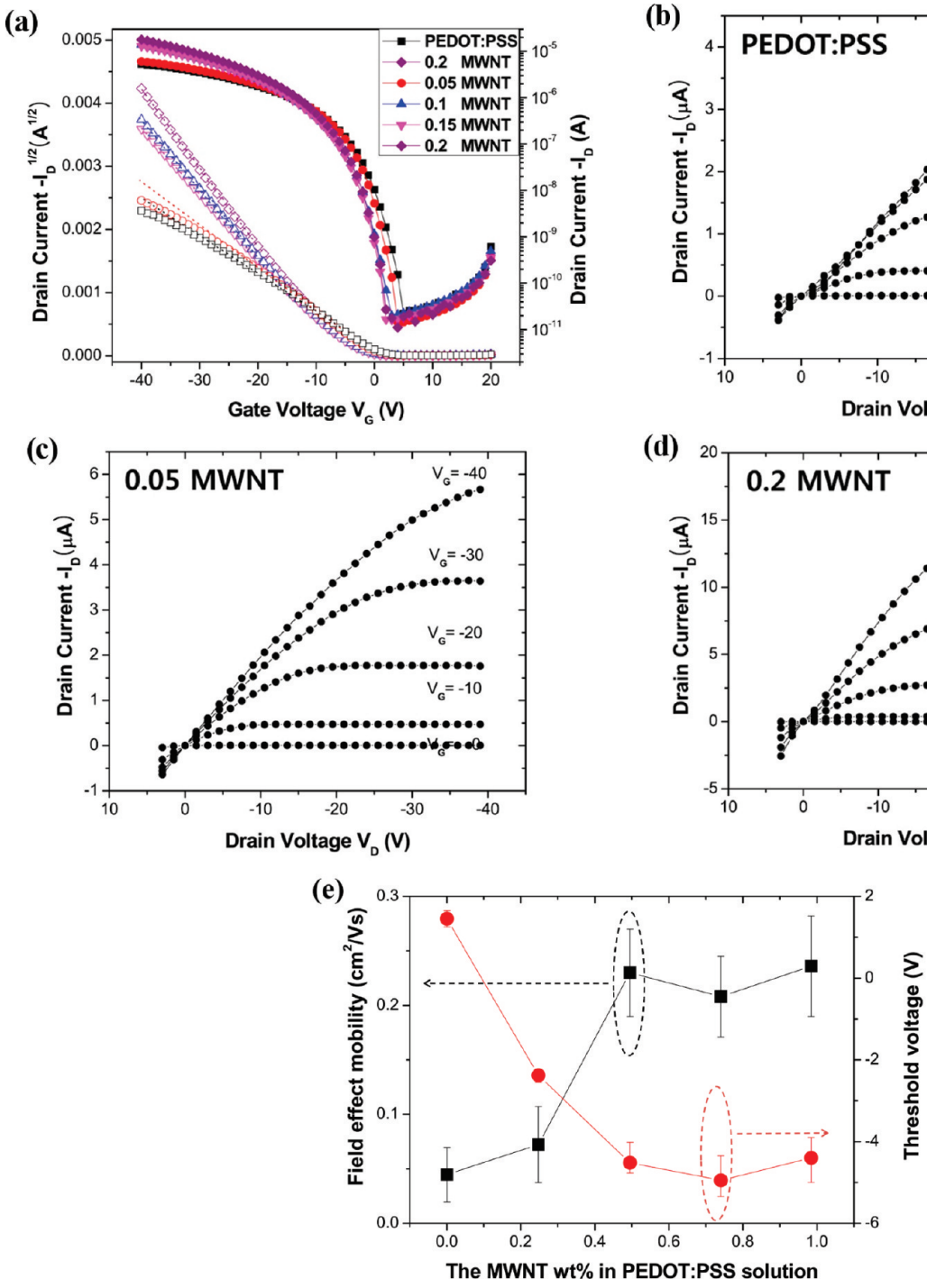

FIGURE 5. (a) Transfer and (b–d) output characteristics of the pentacene TFT with MWNT/PEDOT:PSS S/D electrodes and (e) the field-effect mobility and threshold voltage as a function of the MWNT loading in the PEDOT:PSS solution.

$$I_{DS} = \frac{WC_i}{2L}(V_G - V_T)^2\mu \qquad (2)$$

where I_{DS} is the drain current at specific gate voltage (V_G), W is the channel width, L is the channel length, V_{th} is the threshold voltage, μ is the carrier field effect mobility and C_i is the capacitance per unit area of the gate insulator (C_i of 300 nm thick SiO_2 was measured to be 10 nF/cm^2). Table 1 shows the characteristics (field-effect mobility, on/off current ratio, and threshold voltage) of pentacene TFTs obtained from the transfer characteristics in Figure 5a. The pentacene TFT with PEDOT:PSS and 0.05 MWNT composite film as a S/D electrode showed a low field-effect mobility of μ = 0.0447 and 0.0723 cm^2/(V s), respectively with on/off ratios about ~1 × 10^5. The slope of the square root drain current versus gate voltage was not exactly linear at high gate voltage due to the high resistance of PEDOT:PSS and 0.05 MWNT composite film as shown in the transfer and output characteristics of Figure 5a–c. On the other hand, the pentacene TFTs with 0.1 MWNT, 0.15 MWNT and 0.2 MWNT S/D

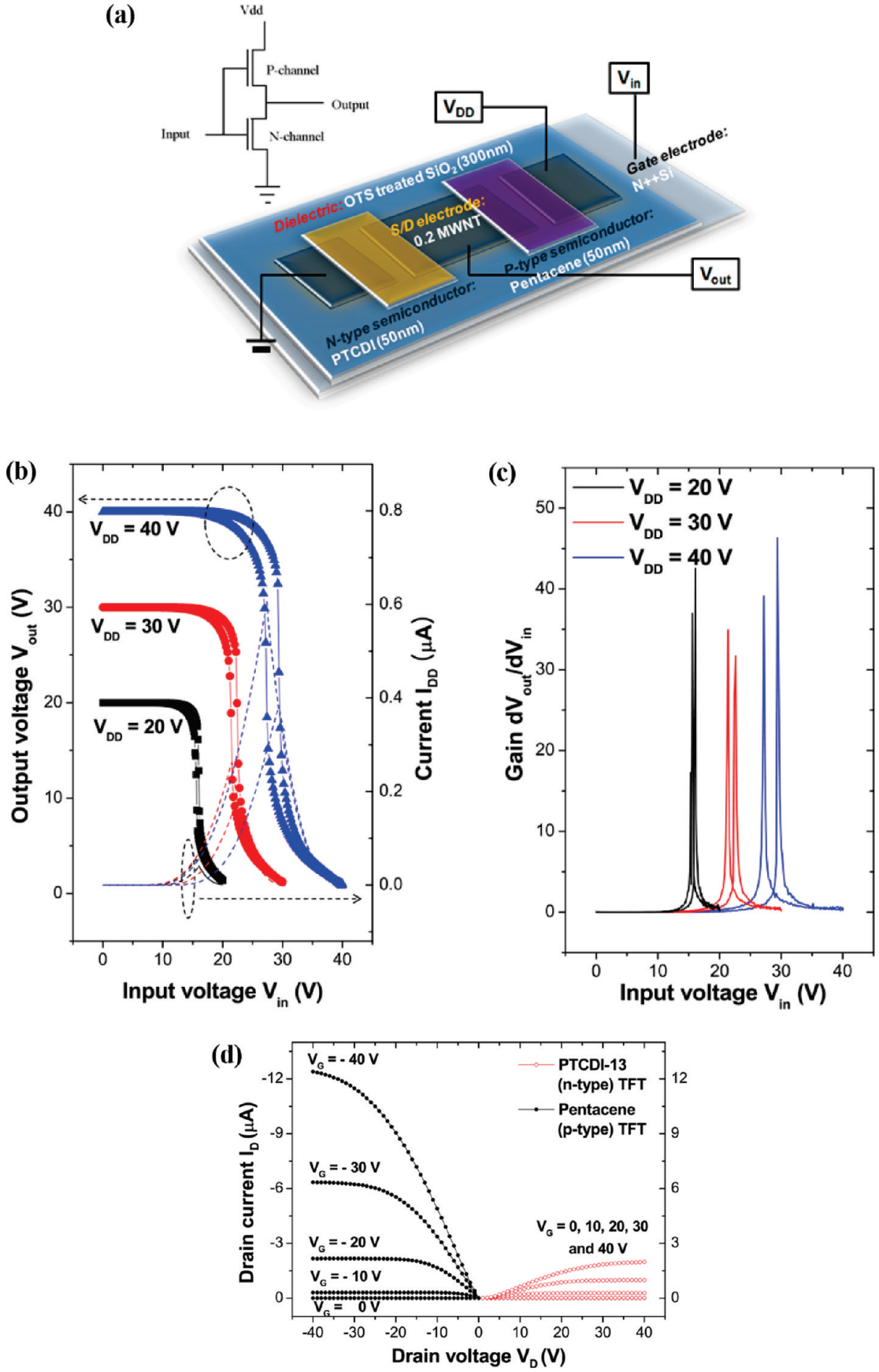

FIGURE 6. (a) Characteristic curve of the complementary inverter with 0.2 MWNT/PEDOT:PSS S/D electrode, (b) the voltage transfer characteristics, (c) DC gain with various V_{DD} values and (d) the comparative output characteristics of p- and n-type TFTs.

electrodes showed a high mobility of ~0.2 $cm^2/(V\ s)$ and on/off ratio of ~5×10^5. The threshold voltage of these TFTs was higher at a voltage near −4.5 V compared to the TFTs with PEDOT:PSS ($V_{th} = 1.45$ V) and 0.05 MWNT ($V_{th} = -2.38$ V) S/D electrode because there was no drain current loss at the high gate voltage as shown in panels d and e in Figure 5.

Because the MWNT/PEDOT:PSS film showed high performance as a S/D electrode of pentacene TFT, the complementary inverter with 0.2 MWNT composite film as a S/D electrode was also fabricated and characterized. As shown in Figure 6b, the complementary inverters showed good output voltage (V_{out})−input voltage (V_{in}) characteristics. The V_{out} stayed close to V_{DD} at low V_{in} and abruptly dropped to 0 V above the specific V_{in} (24−26). This behavior was from the complementary turning on and off operation of p-type (pentacene) and n-type (PTCDI-C13) TFTs. The DC gains (dV_{out}/dV_{in}) as a function of V_{in} was plotted in Figure 6c and they were higher than >30. On the other hand, asymmetry in the $V_{out}-V_{in}$ characteristics such as a positive shift of inverter threshold voltage and a low voltage drop near $V_{out} = 0$ V were observed due to the difference in the saturation mobility between p-type TFT and n-type TFT. The output characteristics were compared in Figure 6d (25, 26).

4. CONCLUSIONS

MWNT/PEDOT:PSS films with various MWNT loading were prepared and film properties as a function of the MWNT were studied. The film properties including the work function, morphology and sheet resistance highly depended on the MWNT/PEDOT:PSS composition. Despite of the low work function (4.8−4.7 eV), the pentacene TFT with MWNT/PEDOT:PSS S/D electrode showed much higher performance (mobility of ~0.2 $cm^2/(V\ s)$ and on/off ratio of ~5×10^5) compared to the PEDOT:PSS S/D electrode (~ 0.05 $cm^2/(V\ s)$, 10^5) owing to the high conductivity of MWNT/PEDOT:PSS films. The complementary inverters with 0.2 MWNT S/D electrode exhibited excellent inverter characteristics including the high gain value of greater than 30.

Acknowledgment. This research was supported by the Korea Research Foundation (KRF) through the National Research Laboratory Project and Polymer Gel Cluster group of the Korean government (Grant No. 2010-0018087). Dong-Jin Y. is grateful to Y. K. Lee (researcher at POSTECH) for supporting photolithography.

Note Added after ASAP Publication. In the original version of this paper published on January 4, 2011, there were incorrect values given in Table 1 and in the Results & Discussion section. The corrected version was published on January 6, 2011.

REFERENCES AND NOTES

(1) Rhee, S. W.; Yun, D. J. *J. Mater. Chem* **2008**, *18*, 5437.
(2) Ma, H.; Yip, H. L.; Huang, F.; Jen, A. K. Y. *Adv. Funct. Mater.* **2010**, *20*, 1.
(3) Murakami, T. N.; Gratzel, M. *Inorg. Chim. Acta* **2008**, *361*, 572.
(4) Steirer, K. X.; Berry, J. J.; Reese, M. O.; Hest, M. F. V.; Miedaner, A.; Liberatore, M. W.; Collins, R. T.; Ginley, D. S. *Thin Solid Films* **2009**, *517*, 2781.
(5) Geng, H. Z.; Kim, K. K.; So, K. P.; Lee, Y. S.; Chang, Y.; Lee, Y. H. *J. Am. Chem. Soc.* **2007**, *129*, 7758.
(6) Tantang, H.; Ong, J. Y.; Loh, C. L.; Dong, X.; Chen, P.; Chen, Y.; Hu, X.; Tan, L. P.; Li, L. J. *Carbon* **2009**, *47*, 1867.
(7) Geng, H. Z.; Kim, K. K.; Song, C.; Xuyen, N. T.; Kim, S. M.; Park, K. A.; Lee, D. S.; An, K. H.; Lee, Y. S.; Chang, Y.; Lee, Y. J.; Choi, J. Y.; Benayad, A.; Lee, Y. H. *J. Mater. Chem.* **2008**, *18*, 1261.
(8) Jackson, R. K.; Munro, A.; Nebesny, K.; Armstrong, N.; Graham, S. *ACS Nano* **2010**, *4*, 1377.
(9) Hatton, R. A.; Blanchard, N. P.; Tan, L. W.; Latini, G.; Cacialli, F.; Silva, S. R. P. *Org. Electron.* **2009**, *10*, 388.
(10) Ou, E. C.; Hu, L.; Raymond, G. C. R.; Soo, O. K.; Pan, J.; Zheng, Z.; Park, Y.; Hecht, D.; Irvin, G.; Drzaic, P.; Gruner, G. *ACS Nano* **2009**, *3*, 2258.
(11) Yu, W. J.; Kang, B. R.; Lee, I. H.; Min, Y. S.; Lee, Y. H. *Adv. Mater.* **2009**, *21*, 1.
(12) Chang, C. H.; Chien, C. H.; Yang, J. Y. *Appl. Phys. Lett.* **2007**, *91*, 083502.
(13) Najafi, E.; Kim, J. Y.; Han, S. H.; Shin, K. *Colloid Surf., A* **2006**, *284*, 373.
(14) Kim, K. K.; Yoon, S. M.; Choi, J. Y.; Lee, J.; Kim, B. K.; Kim, J. M.; Lee, J. H.; Paik, U.; Park, M. H.; Yang, C. W.; An, K. H.; Chung, Y.; Lee, Y. H. *Adv. Funct. Mater.* **2007**, *17*, 1775.
(15) Ham, H. T.; Choi, Y. S.; Chung, I. J. *J. Colloid Interface Sci.* **2005**, *286*, 216.
(16) Datsyuk, V.; Kalyva, M.; Papagelis, K.; Parthenios, J.; Tasis, D.; Siokou, A.; Kallitsis, I.; Galiotis, C. *Carbon* **2008**, *46*, 833.
(17) Hu, C. G.; Wang, W. L.; Liao, K. J.; Liu, G. B.; Wang, Y. T. *J. Phys. Chem. Solids* **2004**, *65*, 1731.
(18) Lim, S. C.; Jo, C. S.; Jeong, H. J.; Shin, Y. M.; Lee, Y. H.; Samayoa, I. A.; Choi, J. *Jpn. J. Appl. Phys.* **2002**, *41*, 5635.
(19) Wu, T. M.; Lin, Y. W.; Liao, C. S. *Carbon* **2005**, *43*, 734.
(20) Chen, Y.; Kang, K. S.; Han, K. J.; Yoo, K. H.; Kim, J. *Synth. Met.* **2009**, *159*, 1701.
(21) Groenendaal, L.; Jonas, F.; Feitag, D.; Pielartzik, H.; Reynolds, J. R. *Adv. Mater.* **2000**, *12*, 482.
(22) Hwang, J.; Amy, F.; Kahn, A. *Org. Electron.* **2006**, *7*, 387.
(23) Jonsson, S. K. M.; Birgerson, J.; Crispin, X.; Greczynski, G.; Osikowicz, W.; Gon, A. W. D.; Salaneck, W. R.; Fahlman, M. *Synth. Met.* **2003**, *139*, 1.
(24) Walser, M. P.; Kalb, W. L.; Mathis, T.; Brenner, T. J.; Batlogg, B. *Appl. Phys. Lett.* **2009**, *94*, 053305.
(25) Jang, J. Y.; Nam, S.; Chung, D. S.; Kim, S. H.; Yun, W. M.; Park, C. E. *Adv. Func. Mater.* **2010**, *20*, 2611.
(26) Smith, J.; Bashir, A.; Adamopoulos, G.; Anthony, J. E.; Bradley, D. D. C.; Hamilton, R.; Heeney, M.; McCulloch, I.; Anthopoulos, T. D. *Adv. Mater.* **2010**, *22*, 3598.

AM1008375